Research on Motion Distortion Correction Method of Intelligent Vehicle Point Cloud Based on High Frequency Inertial Measurement Unit

Yuqiong Wang, Tianqi Gu, Binbin Sun, Mengxue Xie, Song Gao and Ke Sun

Abstract—**Environment perception is the basis of intelligent driving and the premise of realizing path planning and vehicle controlling. Among them, obstacle detection is the key for environmental perception. In order to cope with the issue of point cloud movement distortion in traditional obstacle detection algorithms, experimental lidar and IMU are first introduced in this paper. On this basis, the lidar coordinate system, the vehicle coordinate system and the relationship of coordinate conversion between them is established, and the point cloud data in the lidar coordinate system is converted into the vehicle coordinate system. In addition , the principle of point cloud motion distortion and its influence on obstacle detection is analyzed. Furthermore, a point cloud motion distortion correction method combining high- frequency IMU is designed to compensate the inter-frame motion of lidar and correct the point cloud motion distortion. Finally, a real vehicle test and verification is carried out. The test results show that, first, the proposed point cloud motion distortion correction method is effective, which can make the collected point cloud data reflect the real environment information as accurately as possible, and the point cloud motion distortion rate drops from the maximum value of 20.38% to 5%. The distortion rate is controlled within 5%. Second, the method can also meet the real-time requirements of intelligent vehicles.**

Index Terms—**intelligent vehicle, environmental perception, obstacle detection, point cloud motion distortion**

Manuscript received July 6, 2022; revised January 14, 2023. This work was supported in part by the Innovation team project of "Qing-Chuang science and technology plan" of colleges and universities in Shandong Province 2021KJ083, the Major Innovation Projects in Shandong under Grant 2020CXGC010405 and 2020CXGC010406, the National Natural Science Foundation Project of China under Grant 51805301 and 52102465, the Postdoctoral Science Foundation of China and Shandong under Grant 2020M680091 and 202003042.

Yuqiong Wang is a doctoral student of School of Transportation and Vehicle Engineering, Shandong University of Technology, Zibo, 255000 PR China. (e-mail: wangyuqiong@sdut.edu.cn).

Tianqi Gu is a graduate student of School of Transportation and Vehicle Engineering, Shandong University of Technology, Zibo, 255000 PR China. (e-mail: tianqi.gu@outlook.com).

Binbin Sun is a Professor of School of Transportation and Vehicle Engineering, Shandong University of Technology, Zibo, 255000 PR China. (corresponding author to provide phone: 86-13708941464; e-mail: sunbin_sdut@126.com).

Mengxue Xie is a graduate student of School of Transportation and Vehicle Engineering, Shandong University of Technology, Zibo, 255000 PR China. (e-mail: xmx233626897@163.com).

Song Gao is a Professor of School of Transportation and Vehicle Engineering, Shandong University of Technology, Zibo, 255000 PR China. (e-mail: gaos546@126.com).

Ke Sun is a graduate student of School of Transportation and Vehicle Engineering, Shandong University of Technology, Zibo, 255000 PR China. (e-mail: sk2019_sdut@163.com).

I. Introduction

Intelligent vehicles have become a research hotspot in the field of vehicle engineering and a new driving force for the rapid growth of automobile industry, as well as will be the trend of the development of automobile technology in the future [1]. The intelligent vehicle system is composed of four parts: environmental perception, positioning, path planning and control. It is a comprehensive intelligent system [2]. The environmental perception system obtains the information of surrounding environment through the perception sensor carried by the intelligent vehicle, which provides a reliable basis for the subsequent positioning and path planning of the intelligent vehicle [3]. In order to realize the omnidirectional and redundant sensing of the surrounding environment, most intelligent vehicles are equipped with sensors such as lidar, camera, millimeter wave radar and ultrasonic radar [4]. Whether environmental perception technology is perfect will directly affect whether intelligent vehicles can run safely in road traffic, which is of great significance and theoretical research value to promote the development of intelligent vehicles.

Obstacle detection is an important part of environmental perception. It detects obstacles from a large number of scattered and disordered point cloud data through operations such as point cloud filtering, ground segmentation and clustering [5]. In recent years, common obstacle detection algorithms in the field of 3D lidar target detection include single-frame-based algorithms, multisensor-fusion, continuous multi-frame-based algorithms, and deep learning algorithms [6-8]. A frame of point cloud data obtained by a rotation of the lidar is not in the same coordinate system. If these data are directly used for subsequent target detection, point cloud motion distortion will occur [9].

In order to remove the movement distortion of point cloud, one method is to obtain the data without distortion when the vehicle is stationary through frequent stops, so as to obtain more accurate point cloud information. However, this method does not conform to the actual driving operation [10]. Some scholars also proposed that the vehicle should be assumed to be moving at uniform speed within a frame point cloud cycle, and then the data of motion distortion is removed [11]. However, in the actual traffic environment, it is impossible for the vehicle to be at a constant speed state all the time. There are also scholars who register the feature points in the point cloud data of adjacent frames, solve the motion between frames, and then remove the motion distortion. The extraction of feature points in this method is

too complicated, the algorithm takes a long time to process, and it cannot meet the real-time requirements of intelligent vehicles [12].

Therefore, this paper studies and proposes a method of fusing high- frequency IMU to correct the motion distortion of point clouds. In the first place, the first part of the article introduces experimental lidar and IMU. The second part discusses the point cloud data coordinate transformation in detail. In the third part, the distortion of point cloud motion is analyzed. Furthermore, the point cloud motion distortion correction method combining high frequency IMU is designed in the fourth part. Finally, experimental verification and data analysis has been carried out.

II. Introduction of Lidar and Inertial Measurement Unit (IMU) for Experiments

In this study, Velodyne HDL-32E lidar was used to detect and track obstacles around intelligent vehicles. It is a mechanical rotating 3D lidar. The internal rotating parts make the laser rotate 360 degrees around the axis continuously, so as to obtain rich point cloud information of the surrounding environment in real time. The Velodyne HDL-32E lidar is capable of firing 32 laser beams at the same time. Each beam has a vertical angular resolution of 1.33° and a horizontal angular resolution of 0.16° . It can obtain more than 700,000 points per second with a measurement accuracy of less than 2cm. Table I gives the main technical indexes of lidar.

Table I Main technical specifications of Lidar

Property	Velodyne HDL-32E
Laser beam	32 lines
Measuring distance	80m-100m
Error +/-cm	±2cm
Horizontal viewing angle	360°
Vertical viewing angle	+10.67°~ -30.67°
Vertical angular resolution	1.33°
Horizontal angular resolution	0.16°
Rotation rate	5-20Hz (10Hz)
Laser wavelength	903nm safety Class1
Output	0.7 million points/second
Weight	1Kg(without cable)
Size	149.86mm*85.3mm
Power	12v@2Amps

As shown in Fig. 1, it is a schematic diagram of the state quantity output of the IMU sensor. IMU consists of three accelerometers and three gyroscopes. Accelerometers measure acceleration information according to Newton's second law. When the speed and position is known at the initial moment, the change of velocity can be obtained by combining the acceleration once, and the change of displacement can be obtained by the second integration. The working principle of the gyroscope is to indirectly measure the angular velocity information by measuring the Coriolis force of the object.

In this study, velocity and angle has been calculated by combining IMU acceleration and angular velocity data. Nevertheless, IMU is merely suitable for integration in a short period of time, and requires integrating with GPS navigation system for positioning, because the integration error will gradually increase with time. The BDFS integrated navigation system was used in this study and the automotive IMU is integrated inside. Ensure that the installation plane of the integrated navigation equipment is horizontal when installing it. Additionally, the Y axis of the shell system marked on the equipment should be kept in the same line with the Y axis direction of the carrier system. The performance index parameters of IMU are given in Table II.

Table II IMU performance index

IMU Performance Indicators	Gyroscope	Accelerometer
Measuring range	±300°/s	±10g
Resolution	16 bit	12 bit
Zero bias stability	≤0.05°/s	≤1mg
Scale factor nonlinearity	0.02%FS	0.2%FS
Zero bias repeatability	0.004°/s(1σ)	1.0mg

III. Coordinate Transformation of Point Cloud Data

A. Coordinate System Definition

(1) Lidar Coordinate System

The definition of the Velodyne 32-line lidar coordinate system is that the origin O is located in the center of the laser radar, the X-axis points horizontally to the right of the device, and the Y-axis points straight ahead perpendicular to the X-axis. Since the X, Y, and Z axes correspond to the right hand coordinate system, the positive direction of the Z axis is vertical and upward perpendicular to the XY plane (the Z axis is the rotation axis when the lidar works). The lidar coordinate system is shown in Fig. 2.

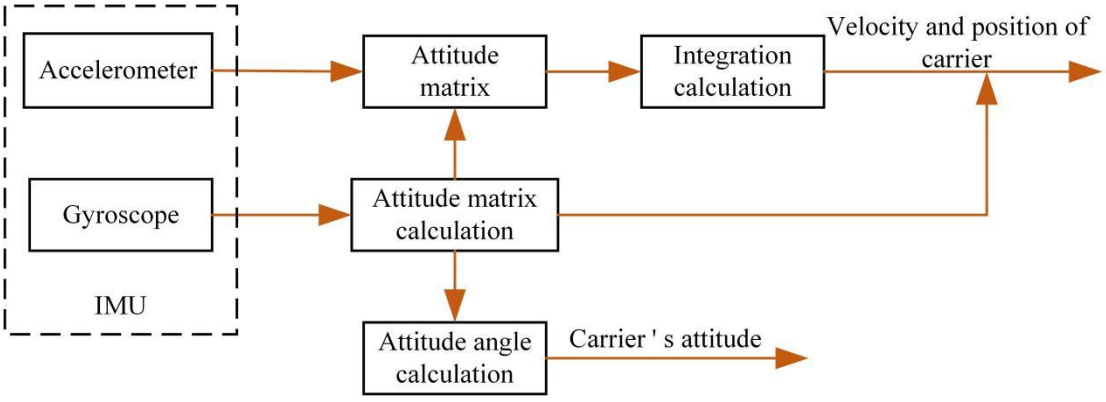

Fig. 1 Status output diagram of IMU sensor

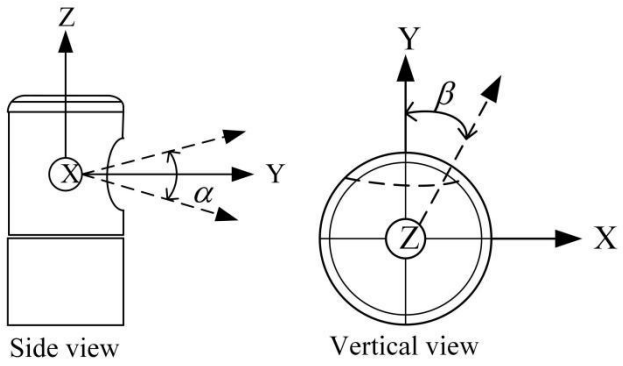

Fig. 2 Lidar coordinate system

The laser radar obtains the original scanning data in the polar coordinate system and transmits it through the Ethernet in the form of UDP packets. The returned laser point information includes echo distance, vertical angle and horizontal angle. In order to facilitate data processing, it is necessary to establish a Cartesian coordinate system to analyze the original data and convert it into three-dimensional coordinate information to prepare for subsequent point cloud processing. The conversion of lidar original data is shown in Fig. 3.

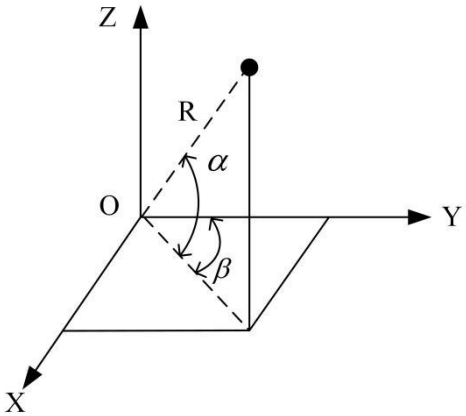

Fig. 3 Conversion of Lidar raw data

Through equation (1), the original point cloud data in the polar coordinate system is transformed into three-dimensional coordinates in the Cartesian coordinate system.

$$\begin{cases} x = R * \cos\alpha * \sin\beta \\ y = R * \cos\alpha * \cos\beta \\ z = R * \sin\alpha \end{cases} \tag{1}$$

Here, R is the echo distance of the point, α is the vertical angle, the vertical angle between each harness is fixed and is given by the radar user manual, β is the horizontal angle of the emission harness, obtained from the angle encoder on the rotary axis.

After converting point clouds data to lidar Cartesian coordinate system, a set of multi-dimensional points is obtained, which is collectively called point clouds. Its data structure is represented by equation (2).

$$P = (p_1, p_2, p_3 \cdots p_i) \tag{2}$$

In the formula above, $p_i = (x_i, y_i, z_i, I_i), (x_i, y_i, z_i)$ is the three-dimensional position coordinate information of the point, I_i is the reflection intensity information.

(2) Vehicle Coordinate System

The definition of the vehicle coordinate system: the origin O is located in the center of the rear axle of the vehicle, the positive direction of the X_V axis points horizontally to the right of the vehicle, the Y_V axis points directly in front of the vehicle, and the Z_V axis points perpendicular to the X_VY_V plane. Fig. 4 is a schematic diagram of vehicle coordinate system.

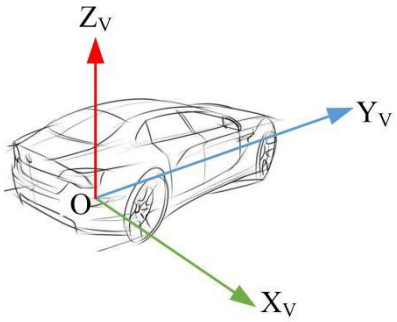

Fig. 4 Vehicle coordinate system

B. Conversion between lidar coordinate system and vehicle coordinate system

Point cloud data based on the laser coordinate system cannot be used for target detection directly. The position information relative to the vehicle coordinate system needs to be obtained through coordinate transformation first to ensure the accurate target detection of intelligent vehicles. The transformation between the two coordinate systems is accomplished by a rotation matrix and a translation vector in the order of rotation and translation. The transformation equation between coordinate systems is shown in equation (3).

$$\begin{bmatrix} x_v \\ y_v \\ z_v \end{bmatrix} = R \begin{bmatrix} x \\ y \\ z \end{bmatrix} + \begin{bmatrix} t_x \\ t_y \\ t_z \end{bmatrix} \tag{3}$$

Where (x_v,y_v,z_v) represents points in the vehicle coordinate system, (x,y,z) is the point in the lidar coordinate system, (t_x,t_y,t_z) is the translation vector and R is the rotation matrix.

The rotation matrix is determined by the *roll*, *pitch* and *yaw* about X, Y and Z axes respectively. The positive or negative euler angles are judged according to the rule of the right hand, the right hand clenched, the coordinate system through the palm, four fingers pointing in the positive direction, otherwise it is the opposite direction. The total rotation matrix is different in different rotation orders. The rotation order used in this paper is first around X, then around Y, and finally around Z axis, and then the left multiplication of rotation. The final rotation around each axis is obtained by formula (4), (5), and (6).

$$R_x = \begin{bmatrix} 1 & 0 & 0 \\ 0 & \cos(roll) & -\sin(roll) \\ 0 & \sin(roll) & \cos(roll) \end{bmatrix} \tag{4}$$

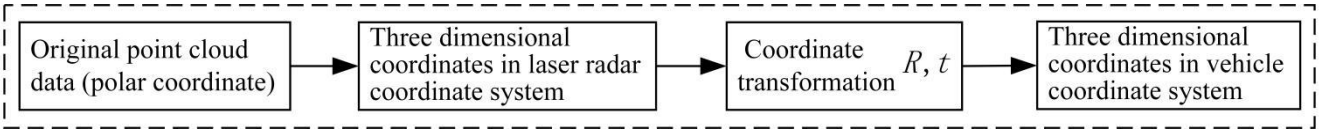

Fig. 5 Point cloud data conversion

$$R_y = \begin{bmatrix} \cos(pitch) & 0 & \sin(pitch) \\ 0 & 1 & 0 \\ -\sin(pitch) & 0 & \cos(pitch) \end{bmatrix} \quad (5)$$

$$R_z = \begin{bmatrix} \cos(yaw) & -\sin(yaw) & 0 \\ \sin(yaw) & \cos(yaw) & 0 \\ 0 & 0 & 1 \end{bmatrix} \quad (6)$$

According to formula (4), (5) and (6), the total rotation matrix R can be calculated by Formula (7).

$$R = R_z * R_y * R_x \quad (7)$$

The translation vector (t_x,t_y,t_z) represents the positional relationship among the origins of the two coordinate systems, and is directly calculated from the difference between the origins of the two coordinate systems. After the above steps, the original point cloud data is converted from the lidar coordinate system to the vehicle coordinate system. The specific conversion process is shown in Fig. 5.

IV. Distortion Analysis of Point Cloud Motion

As shown in Fig. 6, during lidar measurement, the laser point data cannot be obtained instantaneously due to vehicle movement, which leads to the problem that the data in one frame point cloud are not in the same coordinate system, resulting in point cloud movement distortion. For example, in this experiment, it takes 0.1 seconds for lidar to collect a frame of point cloud data. When the vehicle runs in a straight line at the speed of 60km/h, the position deviation between the first point and the last point in a frame of point cloud will reach about 1.6 meters. When the vehicle is stationary and moving, the point cloud data of one frame are different. The obstacles in front are getting closer and the obstacles in the rear are getting farther and farther, which may eventually lead to problems in obstacle detection and vehicle positioning.

As shown in Fig. 7(a), the target to be detected is in the front right of the intelligent vehicle, which is in a static state. The length of the target obtained by lidar scanning is AB.

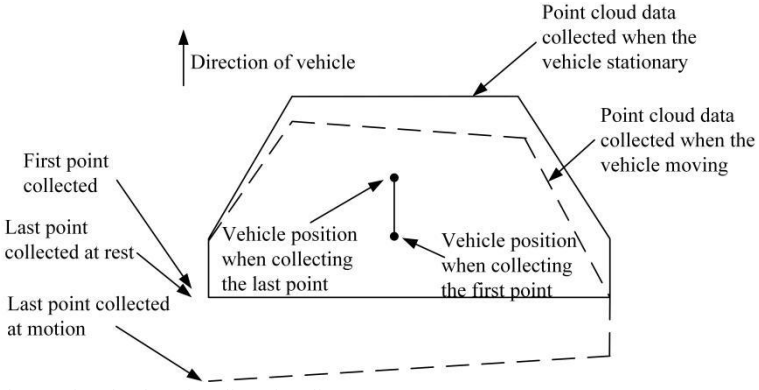

Fig. 6 Point cloud motion distortion diagram

How ever, when the smart car moves straight ahead, when the lidar scans the last point on the target, the position of the vehicle moves forward for a certain distance relative to the stationary vehicle, and the actual length of the target obtained by scanning is CD. Obviously, the length of CD is less than the length of AB, that is, when the vehicle runs in a straight line, due to motion distortion, the detected target length is smaller than that when the vehicle is stationary without distortion.

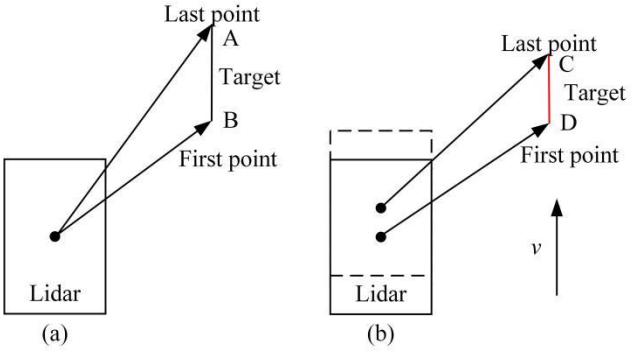

Fig. 7 Difference between stationary and moving vehicle detection targets

As shown in Fig. 8, the target to be detected is located directly in front of the vehicle. As the vehicle moves forward, the distance between the target and the lidar gradually decreases, and the distance between a frame of point cloud data collected by the lidar and the vehicle is different. The red target scanned by the lidar of a moving vehicle is distorted in shape compared to the same target scanned when the vehicle is stationary.

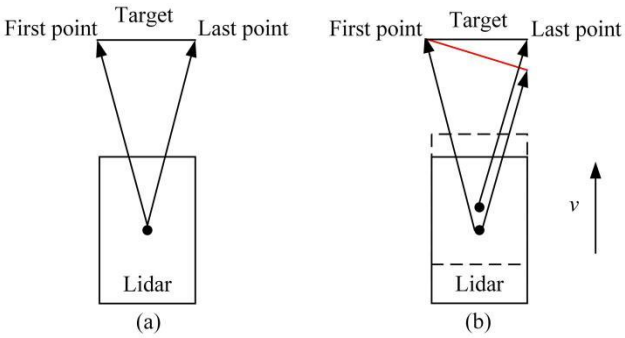

Fig. 8 Difference between stationary and moving vehicle detection targets

When the smart car travels in a straight line, the motion of the lidar causes the length and width of the target to change and the shape to deform. Similarly, when the vehicle turns to drive, the length, width and shape of the object to be detected in front of it will also change. The lidar collects data by rotating clockwise. When the vehicle turns right, the detected target size will decrease, and when the vehicle turns left, the target size will increase. The point cloud motion distortion not only affects the target detection, but also has a certain impact on the subsequent positioning and planning modules, which reduces the driving safety of the smart car. Therefore, point cloud motion distortion correction is very necessary.

V. Point Cloud Motion Distortion Correction

In this study, the method of fusing high-frequency IMU is used to correct the motion distortion of point cloud. Using a separate thread, receive high-frequency raw data from the IMU in real time. The angle at the current moment is obtained by integrating the rotation angle at the previous moment and the angular velocity during this period. Calculate the actual acceleration by removing the effect of the gravitational acceleration, and then obtain the velocity and position by integrating. Assuming that the smart car accelerates uniformly between the two frames of data before and after the IMU, the position and speed of the vehicle at time t are:

$$\begin{cases} x_t = x_{t-1} + v_{t-1}\Delta t + \frac{1}{2}a\Delta t^2 \\ v_t = v_{t-1} + a\Delta t \end{cases} \tag{8}$$

In the formula, Δt is the time difference between the frame data before and after, x_{t-1} is the position of the vehicle at the previous moment, v_{t-1} is the speed of the vehicle at the previous moment, and a is the actual acceleration

By overlapping the IMU coordinate system with the global coordinate system, the position and speed of the vehicle in the global coordinate system can be obtained. For lidars with lower rotation frequencies, a separate thread is also used to receive data, and the data points $p = (x, y, z)$ are first converted to the vehicle body coordinate system through point cloud data coordinate transformation. Then, solve for the horizontal angle of each laser spot. Lidar scans the surrounding environment by rotating multiple laser beams in the vertical direction around the axis, and stores data in columns. The first and last points in a frame of point cloud data are the points collected at the earliest and latest times. The angle difference between the two points is the actual scanning angle of the lidar. The horizontal angles of the data points at the start and end of the scan are:

$$\begin{aligned} \theta_F &= \arctan\left(\frac{y_1}{x_1}\right) \\ \theta_L &= \arctan\left(\frac{y_n}{x_n}\right) \end{aligned} \tag{9}$$

In the formula, θ_F is the horizontal angle of the first laser point at the beginning of the scan, θ_L is the horizontal angle of the last point at the end of a frame of point cloud scanning, and the difference between the two is the lidar scanning in the point cloud data of the frame. The actual angle of , n represents the total number of laser points in the frame.

From this, the horizontal angle of any point in the point cloud data of this frame can be deduced as:

$$\theta_i = \arctan\left(\frac{y_i}{x_i}\right) \tag{10}$$

Further, the time difference between any point in the frame of point cloud data and the scan start time can be derived.

$$\Delta t_i = \frac{\theta_i - \theta_F}{\theta_L - \theta_F} \times t_{scan} \tag{11}$$

In the formula, Δt_i is the time elapsed between any laser point and the first point, and t_{scan} is the period of one frame of point cloud data.

In order to calculate the motion amount in the process of lidar data acquisition, and then compensate the motion amount, this study obtains the information corresponding to the laser point by performing linear interpolation on the IMU data, and then performs compensation. Specifically, firstly, at the time of the laser point, find the IMU data with the closest distance between the two frames before and after. Further, the interpolation operation obtains the IMU data at the current moment, that is, the position and attitude of the vehicle. As shown in Fig. 9, assuming that the current laser point time is t_i, the IMU data times of the preceding and following frames are respectively t_k and t_{k+1}.

Firstly, the interpolation factor was calculated according to the time-point diagram in Figure 9 and the linear interpolation principle.

$$ratio = \frac{t_{k+1} - t_i}{t_{k+1} - t_k} \tag{12}$$

Further, the position, speed and attitude of the vehicle corresponding to the laser point are calculated from the interpolation factor and the IMU data of the two frames before and after the laser point time.

$$\begin{cases} x_i = (1 - ratio)x_k + ratio * x_{k+1} \\ v_i = (1 - ratio)v_k + ratio * v_{k+1} \\ \varphi_i = (1 - ratio)\varphi_k + ratio * \varphi_{k+1} \end{cases} \tag{13}$$

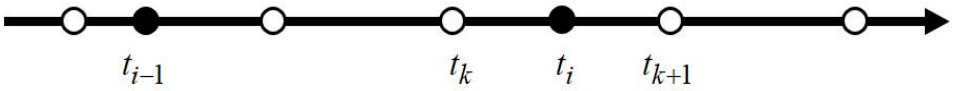

Fig. 9 Relationship between laser point and IMU data time point

In the formula, x_i is the vehicle position corresponding to the laser point time, x_k and x_{k+1} are the vehicle position obtained after two integrations of the IMU acceleration data of the front and rear frames respectively,vi is the vehicle speed corresponding to the laser point time, v_k and v_{k+1} respectively is the vehicle speed obtained after one integration of the IMU acceleration data of the front and rear frames, φ_i is the vehicle attitude corresponding to the laser point time, φ_k and φ_{k+1} are the vehicle attitude obtained after the integration of the IMU angular velocity data of the front and rear frames, respectively, ratio is the interpolation factor.

Finally, according to the motion of the laser point moment and the initial moment in a frame of point cloud, the relative motion transformation between them is calculated. According to the determined time between the laser point and the first point, all laser points are converted to the initial time coordinate system, and then the correction of point cloud motion distortion can be completed.

VI. Experimental verification

As shown in Fig. 10, it is an experimental prototype of a smart car. In order to reduce the occlusion and obtain a larger field of view of the lidar, the Velodyne 32 line lidar is mounted on the roof of the vehicle through a tripod. A Delphi millimeter-wave radar is installed on the front of the bumper, and Mobileye's camera is installed on the front windshield of the car. A GNSS integrated navigation system is installed in the car.

Fig. 10 Experimental vehicle

A. The smart car drives in a straight line, and the target is directly in front of the smart car.

Fig. 11 shows the actual scene diagram of the smart car driving in a straight line and the target is directly in front of the smart car. Fig. 12 shows the comparison of the original point cloud, the distorted point cloud and the corrected point cloud of the measured target. Among them, Fig. 12 (a) is the original point cloud data map obtained when the smart car is stationary. Fig. 12(b) is the pedestrian point cloud data map obtained when the smart car is driving in a straight line. It can be seen from the test results that the point cloud data of the test target is distorted. As shown in Table III, Table IV and Table V, the clustering results of the detected objects and the width variation of the point cloud data of the detected objects are given. Analysis of the data in the table shows that the width of the point cloud data is larger than the original point cloud data's. The point cloud width of the detected target is smaller than the original point cloud width, so the detection result is inaccurate, which will affect the driving safety of the smart car. Fig. 12(c) shows the line point cloud data after the distortion correction method. Table VI presents the changes in the length and width of pedestrian point clouds before and after distortion correction. The experimental results show that the point cloud data distortion correction method proposed in this paper can make the corrected point cloud of the measured object closer to the original point cloud, and the maximum distortion rate is reduced from 20.38 % to 5 % .

Fig. 11 Actual scene

Table III Data of original point cloud

Point cloud information	Pedestrian A	Pedestrian B
Number of point clouds	375	391
Cluster length (m)	0.586	0.591
Cluster width (m)	0.260	0.264
Cluster height (m)	1.689	1.691
Cluster volume (m^3)	0.257	0.263
Detection distance (m)	6.215	6.215

Table IV Data of distorted point cloud

Point cloud information	Pedestrian A	Pedestrian B
Number of point clouds	369	386
Cluster length (m)	0.585	0.590
Cluster width (m)	0.313	0.316
Cluster height (m)	1.681	1.685
Cluster volume (m^3)	0.307	0.314
Detection distance (m)	6.145	6.175

Table V Point cloud data after distortion correction

Point cloud information	Pedestrian A	Pedestrian B
Number of point clouds	371	386
Cluster length (m)	0.585	0.589
Cluster width (m)	0.273	0.276
Cluster height (m)	1.681	1.685
Cluster volume (m^3)	0.268	0.274
Detection distance (m)	6.165	6.185

Table VI Change of point cloud size before and after distortion correction

Point cloud size	Pedestrian A	Pedestrian B
Original length (cm)	58.6	59.1
Distorted length (cm)	58.5	59.0
Corrected length (cm)	58.5	58.9
Original width (cm)	26.0	26.4
Width after distortion (cm)	31.3	31.6
Corrected width (cm)	27.3	27.6

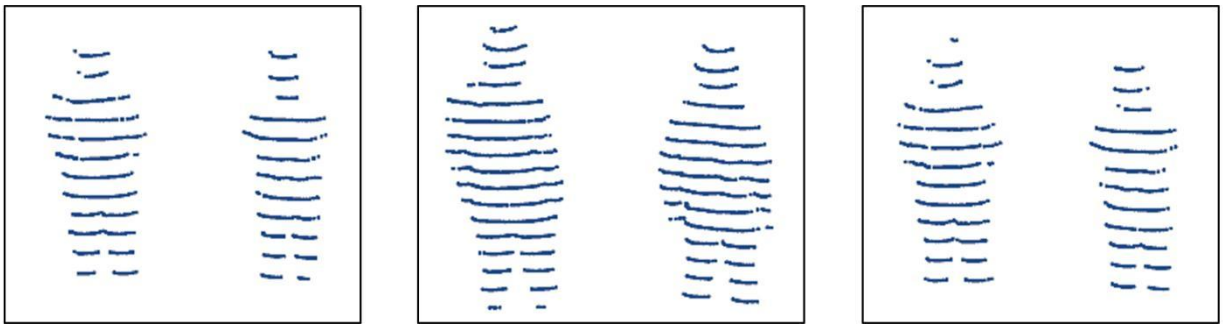

(a) Original point cloud (b) Distorted point cloud (c) Corrected point cloud

Fig. 12 Distortion and correction results of pedestrians in front

B. The smart car drives in a straight line, and the target is in the right front of the smart car

Fig. 13 shows the actual scene diagram of the smart car driving in a straight line and the target in the front right of the smart car. Fig. 14 shows the comparison of the original point cloud, the distorted point cloud and the corrected point cloud of the measured target. Among them, Fig. 14 (a) is the original point cloud data map obtained when the smart car is stationary. Fig. 14(b) is the point cloud data map of the measured target obtained when the smart car is driving in a straight line. It can be seen from the test results that the point cloud data of the test target is distorted. As shown in Table VII, Table VIII and Table IX, the clustering results of the detected objects and the width variation of the point cloud data of the detected objects are given. Analysis of the data in the table shows that the width of the point cloud data of the two tested targets is larger than the original point cloud data's, and the point cloud width of the detected target is smaller than the original point cloud width, and the detection result is inaccurate. Fig. 12(c) shows the line point cloud data after the distortion correction method. Table X shows the changes in the length and width of pedestrian point clouds before and after distortion correction. The experimental results show that the point cloud data distortion correction method proposed in this paper can make the corrected point cloud of the measured object closer to the original point cloud, and the width value of the pedestrian point cloud after correction increases, which is closer to the width of the original point cloud.and the maximum distortion rate is decreased from 17.4 % to 4.5 %.

Fig. 13 Actual scene

Table VII Data of original point cloud

Point cloud information	Pedestrian A	Pedestrian B
Number of point clouds	297	309
Cluster length (m)	0.583	0.588
Cluster width (m)	0.265	0.269
Cluster height (m)	1.689	1.692
Cluster volume (m^3)	0.261	0.268
Detection distance (m)	5.615	5.460

Table VIII Data of distorted point cloud

Point cloud information	Pedestrian A	Pedestrian B
Number of point clouds	252	264
Cluster length (m)	0.586	0.591
Cluster width (m)	0.219	0.223
Cluster height (m)	1.691	1.693
Cluster volume (m^3)	0.217	0.223
Detection distance (m)	5.635	5.488

Table IX Point cloud data after distortion correction

Point cloud information	Pedestrian A	Pedestrian B
Number of point clouds	272	284
Cluster length (m)	0.586	0.591
Cluster width (m)	0.253	0.259
Cluster height (m)	1.691	1.693
Cluster volume (m^3)	0.251	0.259
Detection distance (m)	5.635	5.488

Table X Change of point cloud size before and after distortion correction

Point cloud size	Pedestrian A	Pedestrian B
Original length (cm)	58.3	58.8
Distorted length (cm)	58.6	59.1
Corrected length (cm)	58.6	59.1
Original width (cm)	26.5	26.9
Width after distortion (cm)	21.9	22.3
Corrected width (cm)	25.3	25.9

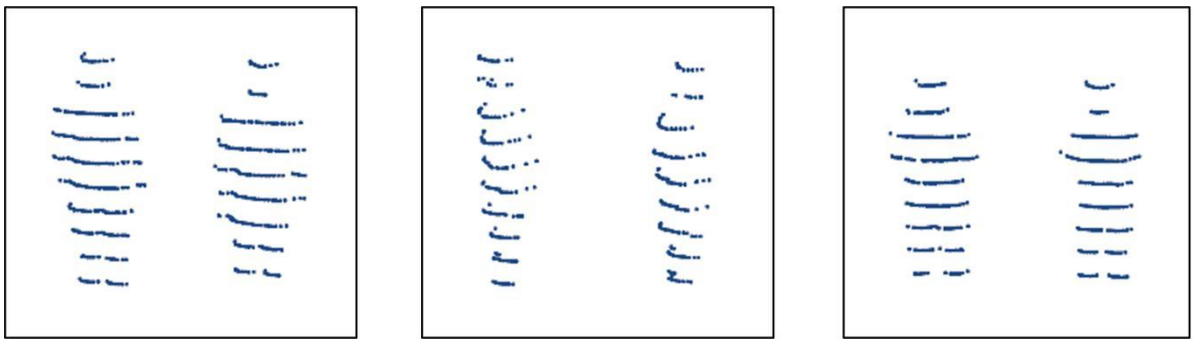

(a) Original point cloud (b) Distorted point cloud (c) Corrected point cloud

Fig. 14 Distortion and correction result of right front pedestrian

VII. Conclusion

In order to solve the problem of point cloud motion distortion caused by lidar accompanied by carrier motion and obtain more realistic point cloud data, this paper studies and proposes a distortion correction algorithm fused with high-frequency IMU data. Through the design of point cloud data coordinate transformation method, the transformation of point cloud data from lidar coordinate system to vehicle coordinate system is realized. By calculating the receiving time of each laser point and the motion transformation relationship of the lidar relative to the initial time, a frame of point cloud data is converted into the same coordinate system, and the motion distortion is removed. The real vehicle test results show that the method has obvious effect of removing distortion, which makes the collected point cloud data reflect the surrounding real environment information as much as possible, the point cloud motion distortion rate is reduced from the maximum value of 20.38 % to 5 %, and the distortion rate is controlled within 5 %. At the same time, the method meets the real-time requirements of smart cars.

References

[1] Zelin Xu, "Research on Smart Car Obstacle Avoidance System," International Core Journal of Engineering, vol. 6, no.5, pp.1-17, 2020.

[2] Zhiqiang Xu, "Analysis of the Development Trend of Smart Car Industry," International Journal of Education and Economics, vol. 1, no.1, pp.78-81, 2018.

[3] Abdallaoui Sara, Aglzim ElHassane, Chaibet Ahmed, et al., "Thorough Review Analysis of Safe Control of Autonomous Vehicles: Path Planning and Navigation Techniques," Energies, vol. 15, no.4, 2022.

[4] D. Mondal, R. Bera, M. Mitra, "Design and Implementation of an IntegratedRadar and Communication System for Smart Vehicle," International Journal of Soft Computing and Engineering (IJSCE), vol. 5, no.6, 2016.

[5] Itu Razvan,Danescu Radu. "Part-Based Obstacle Detection Using a Multiple Output Neural Network," Sensors (Basel, Switzerland), vol. 22, no.12, 2022.

[6] Meng Ziyao,Xu Shengzhi,Wang Lichao, et al., "Defect object detection algorithm for electroluminescence image defects of photovoltaic modules based on deep learning," Energy Science & Engineering, vol. 10, no.3, pp.800-813, 2022.

[7] Tae-Jae Lee, Chul-hong Kim and Dong-Il Dan Cho., "A Monocular Vision Sensor-Based Efficient SLAM Method for Indoor Service Robots," IEEE Trans. Industrial Electronics, vol. 66, no.1, pp.318-328, 2019.

[8] Guo Dongbing, Wang Chunhui, Qi Baoling, et al., "A Study of Correction to the Point Cloud Distortion Based on MEMS LiDAR System," Applied Sciences, vol. 11, no.5, pp.2418-2418, 2021.

[9] A. Nuchter, K. Lingemann, J. Hertzberg, H. Surmann. "6D SLAM with approximate data association" IEEE 12th International Conference on Advanced Robotics, pp.242-249, 2005.

[10] Pan Zihao, Hou Junyi, Yu Lei. "Optimization algorithm for high precision RGB-D dense point cloud 3D reconstruction in indoor unbounded extension area," Measurement Science and Technology, vol. 33, no.5, 2022.

[11] Shuaixin Li, Guangyun Li, Li Wang, et al., "A three-dimensional robust ridge estimation positioning method for UWB in a complex environment," Advances in Space Research, vol. 60, no.12, pp.2763-2775, 2017.

[12] Lin Hui, "Map construction and obstacle detection based on vehicular multi-laser radar," Zhejiang University, 2017.